npg

Defects of protein production in erythroid cells revealed in a zebrafish Diamond–Blackfan anemia model for mutation in *RPS19*

Y Zhang[1,2], J Ear[2], Z Yang[2], K Morimoto[2], B Zhang[1] and S Lin*[,2]

Diamond–Blackfan anemia (DBA) is a rare congenital red cell aplasia that classically presents during early infancy in DBA patients. Approximately, 25% of patients carry a mutation in the *ribosomal protein (RP) S19* gene; mutations in *RPS24*, *RPS17*, *RPL35A*, *RPL11*, and *RPL5* have been reported. How ribosome protein deficiency causes defects specifically to red blood cells in DBA has not been well elucidated. To genetically model the predominant ribosome defect in DBA, we generated an *rps19* null mutant through the use of TALEN-mediated gene targeting in zebrafish. Molecular characterization of this mutant line demonstrated that rps19 deficiency reproduced the erythroid defects of DBA, including a lack of mature red blood cells and *p53* activation. Notably, we found that *rps19* mutants' production of globin proteins was significantly inhibited; however, globin transcript level was either increased or unaffected in *rps19* mutant embryos. This dissociation of RNA/protein levels of *globin* genes was confirmed in another zebrafish DBA model with defects in *rpl11*. Using transgenic zebrafish with specific expression of mCherry in erythroid cells, we showed that protein production in erythroid cells was decreased when either *rps19* or *rpl11* was mutated. L-Leucine treatment alleviated the defects of protein production in erythroid cells and partially rescued the anemic phenotype in both *rps19* and *rpl11* mutants. Analysis of this model suggests that the decreased protein production in erythroid cells likely contributes to the blood-specific phenotype of DBA. Furthermore, the newly generated *rps19* zebrafish mutant should serve as a useful animal model to study DBA. Our *in vivo* findings may provide clues for the future therapy strategy for DBA.
Cell Death and Disease (2014) **5**, e1352; doi:10.1038/cddis.2014.318; published online 24 July 2014

Diamond–Blackfan anemia (DBA; OMIM 205900) is a rare congenital bone marrow failure syndrome characterized by red cell aplasia and reduced or absent erythroid precursors. Most patients are diagnosed with anemia during infancy or in the neonatal period.[1] Additional physical anomalies are present in 30–40% of DBA patients and include thumb, upper limb, craniofacial, heart and kidney malformations, and short stature.[2,3] One current treatment option for DBA is bone marrow transplantation; however, this procedure is limited by shortage of appropriate marrow donors and is associated with the risk of significant complications.[4,5] Therefore, development of drug-based therapeutics for DBA is much needed and desirable.

DBA is a disease associated with ribosome protein mutations. The most common mutations are found in *RPS19* that occurs in ∼25% of DBA patients. Frameshift, splicing sites, intragenic deletions, nonsense, as well as missense mutations have all been identified.[2] Genetic studies have also identified mutations in other ribosomal proteins, including *RPS7* in 1% of patients and *RPL11* and *RPS26* in 6.5%.[6–12] These findings establish DBA as a disorder of ribosomal biogenesis and/or function.

Knockdown of individual ribosomal proteins in human cell lines interferes with pre-rRNA processing and maturation of the large and small ribosome subunits.[13–16] Presumptively impaired ribosome biogenesis should affect all cell types and understanding why ribosomal protein mutations result in red blood cell-specific defects in DBA remains an interesting but challenging question. It is generally believed that the red blood cell defect is attributed to the activation of *p53* in the erythroid lineage caused by ribosomal deficiency. Activation of *p53* in DBA is well established but its role in erythropoiesis is controversial. A study by Dutt *et al.*[17] reported the selective accumulation of *P53* in the erythroid lineage in human hematopoietic progenitor cells after knocking down *RPS14* or *RPS19* by shRNAs. Inhibition of *p53* rescued impaired erythropoiesis in both mouse and zebrafish models of DBA.[18,19] Recently, *p53*-independent pathways are beginning to be revealed and demonstrated to be partially responsible for defective erythropoiesis.[20,21]

Another hypothesis to the red blood cell-specific defects in ribosomal protein mutations is due to a shortage of globin proteins. Because blood cells have such a high demand for globin protein, a high rate of protein translation is required; any defects in ribosomal function and/or biogenesis would, therefore, be more severe in blood cells compared to other cell types. Blood cells also have a greater demand for overall protein synthesis due to their highly proliferative and

[1]Key Laboratory of Cell Proliferation and Differentiation of Ministry of Education, College of Life Sciences, Peking University, Beijing, People's Republic of China and [2]Department of Molecular, Cell & Developmental Biology, University of California Los Angeles, Los Angeles, CA, USA
*Corresponding author: S Lin, Department of Molecular, Cell & Developmental Biology, University of California Los Angeles, Los Angeles, CA 90095, USA. Tel: +01 310 267 4970; Fax: +01 310 267 4971; E-mail: shuolin@ucla.edu
Abbreviations: DBA, Diamond–Blackfan anemia; RP, ribosomal protein; TALEN, transcription activator-like effector nuclease; dpf, days post fertilization; HSC, hematopoietic stem cell; *hbbe1*, hemoglobin beta e1; *hbbe3*, hemoglobin beta e3

differentiating nature. Protein synthesis rate was reported to be reduced in lymphocytes from DBA patients irrespective of *RPS19* mutations.[22] Studies of mouse erythroblasts with ribosomal protein haploinsufficiency revealed impaired translation of specific transcripts essential for erythropoiesis involving internal ribosomal entry site (IRES).[23] In addition, human K562 cells were shown to express alternatively spliced isoforms of *FLVCR1* transcripts, which were affected by expressing shRNA against *RPS19*.[24] Dysfunction of FLVCR1 as a heme exporter in erythroblasts[25] might also play a role in the erythroid defects of DBA in addition to defective translation rate. Furthermore, decreased expression of the key erythroid signaling protein KIT was detected in fetal liver cells of a *RPS19*-deficient mouse, which may contribute to the erythroid failure in DBA.[26] Although much has been discovered utilizing various models of ribosome deficiency, the exact mechanism of erythroid failure in DBA remains largely unknown. More *in vivo* experiments in various models are needed to elucidate the pathogenesis of DBA.

To gain a better understanding of the mechanism leading to the erythroid-specific defects in DBA, we generated two independent lines of *rps19* mutants using transcription activator-like effector nuclease (TALEN)-mediated gene targeting in zebrafish.[27] Genetic knockout of *rps19* resulted in the characteristic erythroid defects similar to DBA including a lack of mature red blood cells and *p53* activation. Interestingly, we observed that *rps19* mutants had significantly reduced production of globin proteins accompanied by either increased or unaffected level of mRNA transcripts. Similarly, this phenomenon was observed in *rpl11* mutant

zebrafish. Furthermore, we observed that protein production in erythroid cells was decreased with either a mutation in *rps19* or *rpl11*. Treatment with L-leucine improved the defect of protein production and partially rescued the anemic phenotype in both *rps19* and *rpl11* mutants. These findings suggest that decreased protein production in red blood cells is likely a key contributing factor to erythroid-specific defect in DBA.

Results

Generation of *rps19* mutant with TALENs. *Rps19* was the first mutated gene identified in human DBA patients.[2] Zebrafish have a single copy of the *rps19* gene that shares over 88% amino acid sequence identity with the human *RPS19* gene. To generate a zebrafish DBA model carrying *rps19* mutation, TALEN target sites were designed at the boundary of the second intron and the third exon of the *rps19* gene (Figure 1a). The left and right TALENs were co-injected in zebrafish embryos at the one-cell stage to induce insertions or deletions (indels) into the *rps19* gene (Figure 1b). This resulted in premature stop codons in the mRNA (Figure 1c). Two independent stable germline mutations of *rps19* were established (Figures 1b and c). Both *rps19* mutant lines displayed a similar phenotype and we chose the first mutant line (noted as 'Mu1' in Figure 1c) for further investigation. Expression analysis of *rps19* mRNA showed >90% reduction in the *rps19* homozygous mutants (Figure 1d) likely due to nonsense-mediated decay of mRNA. Because mutations of *RPS19* in DBA patients include allele
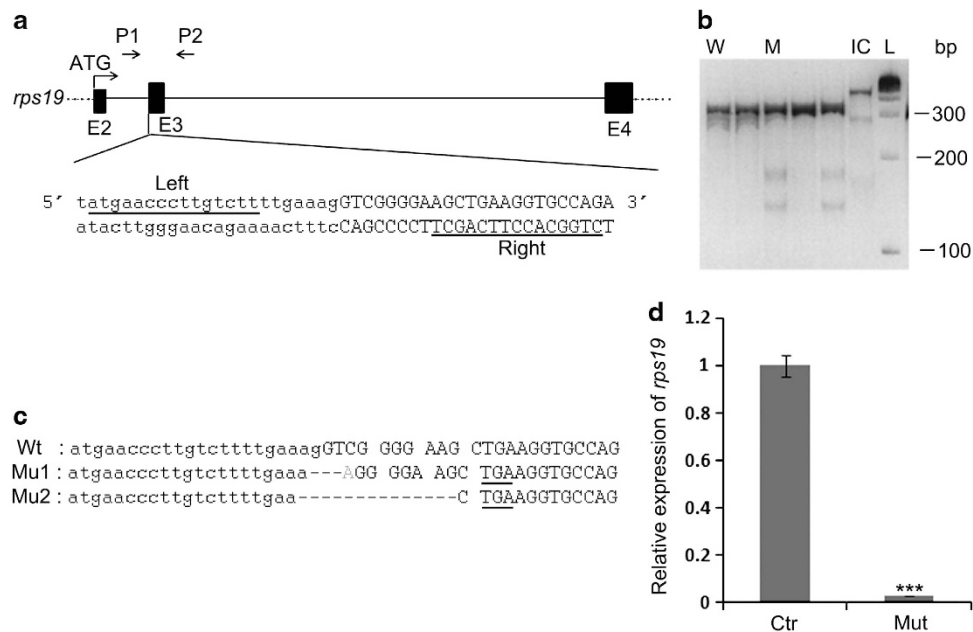

Figure 1 The *rps19* gene in zebrafish is targeted using TALENs. (**a**) Partial structure and sequence of the zebrafish *rps19* gene. The binding sites of the left and right TALENs were underlined. The intron sequence was shown in lowercase and the exon in uppercase. P1 and P2 showed the primer sites for amplification. E2, E3, and E4 represent the second, third, and fourth exon of the *rps19* gene, respectively. (**b**) Identification of mutations by enzyme digestion. PCR products (∼305 bp) were processed with an enzyme that can recognize and cut at mismatch region. The presence of lower bands (∼135 bp and ∼170 bp) suggested a mutation. (**c**) Genomic sequences of the *rps19* mutations. Deletions and insertions were shown in dashes and red letters, respectively. The premature stop codons produced in the two independent mutations were underlined. (**d**) Real-time PCR result showed *rps19* gene expression was reduced by more than 99% in mutant 1. ***$P < 0.001$; Student's *t*-test). W, WT control; M, mutant; IC, internal control; L, DNA Ladder; bp, base pair

deletion, missense mutations, premature stop codons, and internal deletions, we reason that the *rps19* mutant zebrafish would mimic the premature stop codon mutations found in DBA patients.

Phenotypic analysis of *rps19* mutants. *Rps19* homozygous mutants exhibited a similar phenotype as that of *rps19* morphants.[28] At 24 h post fertilization (hpf), *rps19* homozygous mutants showed abnormal development of midbrain–hindbrain boundary (Figure 2a). A curved tail was observed in the mutant embryos at 48 hpf. Compared with siblings, *rps19* mutants exhibited smaller heads and smaller eyes at 3 days post fertilization (dpf). The mutants developed edema (Figure 2a) and died ~5 dpf.

To determine if our *rps19* mutants displayed a DBA-like hematopoietic phenotype, we investigated the expression of multiple primitive and definitive hematopoietic markers using RNA whole-mount *in situ* hybridization. The initial
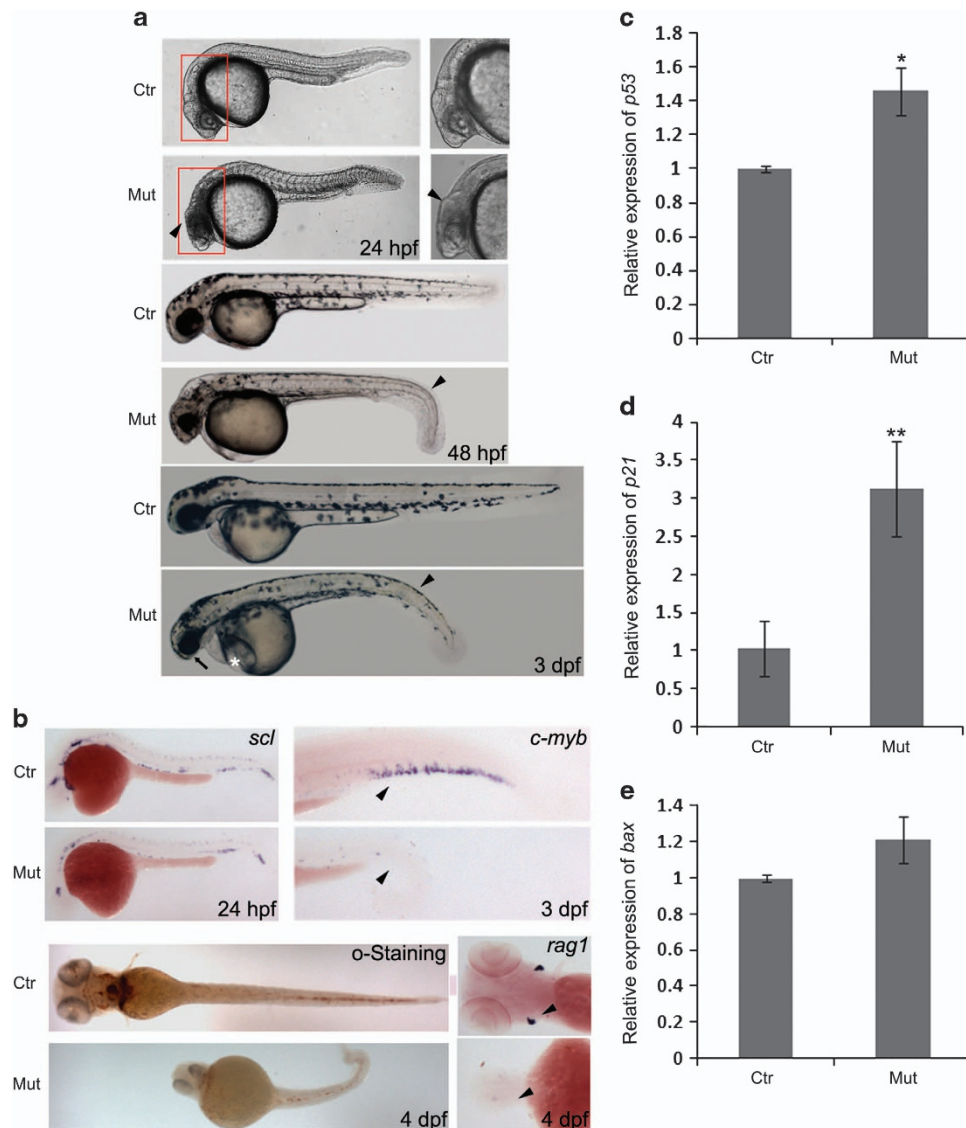
Figure 2 Phenotypic analysis of *rps19* mutants. (**a**) Pictures of embryos at different stages showed the phenotype of *rps19* homozygous mutants. At 24 h post fertilization (hpf), midbrain–hindbrain boundary (MHB) poorly developed in the homozygous mutant embryos (black arrowheads). Boxed areas on the left side were magnified on the right side. Curved tail was observed in homozygous mutant embryos at 48 hpf (black arrowhead). Black arrow showed the smaller head and smaller eyes in homozygous mutant embryos at 3 days post fertilization (dpf). Compared with siblings, the mutant embryos developed edema (white star). The black arrowhead indicated the curved tail in mutant embryos. (**b**) Analysis of hematopoietic defects in *rps19* homozygous mutant embryos. The primitive hematopoietic stem cells (HSCs), marked by *scl* were not affected or slightly less in the mutant embryos at 24 hpf. Both the expression of *c-myb* in definitive HSC at 3 dpf and the hemoglobin stained by *o*-dianisidine staining at 4 dpf were almost disappeared in the mutant embryos. The number of lymphoid cells, marked by *rag1*, was obviously decreased in the mutant at 4 dpf. All the embryos in panel **a** and those for *scl* and *c-myb* probes in panel **b** are lateral view with anterior to the left. The embryos for *o*-dianisidine staining (*o*-staining) are ventral view with anterior to the left. And the embryos for *rag1* probe are dorsal view with anterior to the left. (**c**) Real-time PCR results showed the expression of *p53* was upregulated in *rps19* homozygous mutant embryos. (**d** and **e**) Some of the downstream targets of *p53* were also upregulated in mutant embryos, including *p21*, which is responsible for the induction of cell-cycle arrest and *bax*, which is a mediator of apoptosis. RNA was pooled from 20 embryos at 3 dpf. The results are representative of three independent experiments. *$P < 0.05$; **$P < 0.01$; Student's *t*-test

specification of the primitive hematopoietic cells located in the intermediate cell mass of zebrafish as marked by *scl* expression was not highly affected in *rps19* homozygous mutants at 24 hpf (Figure 2b). However, compared to siblings, expression of the definitive hematopoietic stem cells (HSCs) marker *c-myb* was nearly absent in *rps19* mutants at 3 dpf. *o*-Dianisidine staining revealed that *rps19* mutants had greatly decreased hemoglobin levels at 4 dpf (Figure 2b). This indicated that the number of red blood cells was probably reduced in *rps19* mutants. The reduction of red blood cells may be caused by a decreased cell survival and/or production of definitive HSCs. This is supported by the observation that lymphoid T cells in the thymus, marked by *rag1* expression, were also nearly lacking in *rps19* mutants at 4 dpf (Figure 2b).

Upregulation of the *p53* signaling pathway was reported in the majority of DBA patients, DBA cell culture models, and animal models. As expected, *rps19* deficiency in our mutants led to activation of the *p53* signaling pathway (Figure 2c), including *p53* and its target genes such as the cell-cycle arrest gene, *p21* (Figure 2d), and the apoptotic gene, *bax* (Figure 2e). In addition, similar with the results previously found in *rps29* mutants and other ribosomal protein-deficient models,[29,30] knockdown of *p53* expression could partially rescue mutant phenotype observed in *rps19* homozygous mutants, including the morphological phenotype. Anemic phenotype observed in *rps19* mutants was also partially improved by downregulation of *p53* (Supplementary Figure S1). In conclusion, the *rps19* mutants we generated with TALENs exhibited the characteristic phenotype of DBA patients and should be useful as a model to study pathogenesis of this genetic disease.
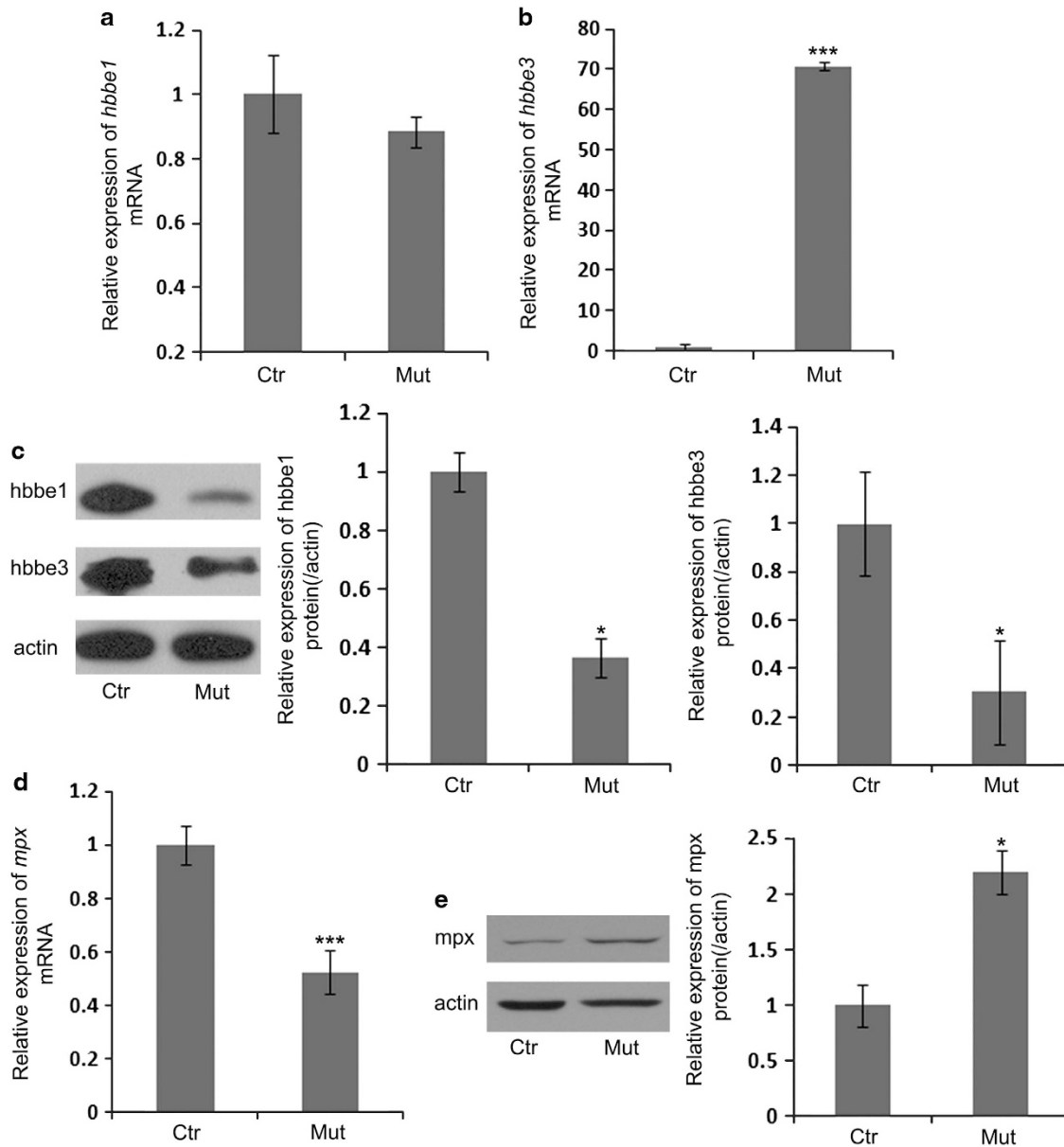
RNA and protein levels of *globin* genes are dissociated in *rps19* mutants. The primary phenotype of DBA is anemia. In the course of characterizing embryonic hemoglobin gene expression in *rps19* mutants we noted that mRNA for *hemoglobin beta e1* (*hbbe1*) was not reduced whereas hemoglobin gene *hbbe3* mRNA was increased by >50-fold (Figures 3a and b). This was somewhat unexpected given that *rps19* mutants lacked globin proteins as revealed by *o*-dianisidine staining. To reconcile this issue, we obtained antibodies specifically recognizing hbbe1 or hbbe3 proteins and quantified globin protein levels by western blot analysis. As expected, we observed significant reduction of protein for both hbbe1 and hbbe3 (Figure 3c), suggesting that there is dissociation of RNA and protein levels for *globin* gene expression in *rps19* mutants. As a control, we analyzed both the mRNA and protein levels for neutrophil marker *mpx*. We detected ~50% less *mpx* mRNA in *rps19* mutants, compared with control embryos (Figure 3d). However, no reduction in mpx protein was detected in *rps19* mutants (Figure 3e). This indicates that the dissociation of RNA and protein production is not ubiquitous but at least partially erythroid cell-specific or globin gene-specific effect.

Protein production in erythroid cells is decreased in *rps19* mutants. Globin is the most abundant protein in red blood cells. The dissociation of *globin* genes' RNA and protein production could result from the deficient protein production in erythroid cells. Alternatively, the dissociation can be due to *globin* gene-specific pathogenesis. In order to address these questions, we generated transgenic zebrafish specifically labeling red blood cells with mCherry. As shown in Figure 4a, zebrafish erythroid-specific regulatory region – locus control region (LCR) as well as a portion of α/β_{a2} bidirectional proximal promoter[31] was cloned into mCherry reporter constructs. Because the dissociation of RNA and protein production was more significant for *hbbe3* than *hbbe1*, we included the 5' untranslated region (UTR) or 3'UTR of *hbbe3* in these constructs (Figure 4a). We observed robust erythroid-specific expression of mCherry in these transgenic embryos, especially in mCherry control line (Supplementary Figure S2). We examined if the globin gene structure has any effects on mCherry expression at the mRNA level and protein level in *rps19* mutants. Real-time PCR results showed equal to more *mCherry* mRNA in mCherry-positive *rps19* mutant embryos than the control embryos at 3 dpf (Figure 4b). However, less mCherry protein, measured through fluorescent intensity, was detected in *rps19* mutants compared to siblings in all three transgenic lines (Figures 4c and d). Interestingly, this RNA/protein production dissociation of *mCherry* was more severe in mCherry control line. Therefore, we observed the dissociation of RNA/protein levels with erythroid-specific mCherry expression regardless of gene structure of *hbbe3*. This indicates that protein production in erythroid cells was inhibited in *rps19* mutants.

RNA and protein levels of *globin* genes are also dissociated in *rpl11* mutants. Previously, a *rpl11* mutant identified with a retrovirus-mediated mutation screening library,[32] has been established as a zebrafish DBA model for its anemic phenotype, *p53* upregulation, and metabolic defects.[30] To determine if the RNA/protein production dissociation for *globin* gene expression was specific to *rps19* mutant or general to DBA-associated ribosomal protein deficiency, we analyzed mRNA expression and protein level in zebrafish *rpl11* mutants. Real-time PCR results showed slightly increased expression of *hbbe1* mRNA in *rpl11* mutant (Figure 5a), while expression of *hbbe3* mRNA was increased by ~50-folds in *rpl11* mutants compared to control embryos (Figure 5b). Furthermore, slightly less *mpx* mRNA was detected in *rpl11* mutants at 3 dpf (Figure 5d). Whole-mount *in situ* hybridization analysis confirmed the real-time PCR as equal to more *hbbe1* mRNA was observed in *rpl11* mutants compared with siblings at 3 dpf (Supplementary Figure S3a). Expression of *hbbe3* mRNA was significantly increased in *rpl11* mutant (Supplementary Figure S3b); *mpx* exhibited similar expression levels between the siblings and *rpl11* mutants (Supplementary Figure S3c). As we discovered in *rps19* mutants, less hbbe1 and hbbe3 proteins were also shown in *rpl11* mutants by western blot analysis (Figure 5c), whereas protein level of *mpx* was comparable between control and *rpl11* mutants (Figure 5e). These findings demonstrated that the RNA/protein production dissociation of *globin* genes without concurrent dissociation seen in the neutrophil cells is likely a common phenomenon shared between multiple ribosome mutations found in DBA.

Figure 3 RNA and protein levels of *globin* genes are dissociated in *rps19* mutants. (**a**) mRNA expression of *globin* gene *hemoglobin beta e1* (*hbbe1*) was not affected or slightly decreased in *rps19* mutant embryos at 3 dpf by real-time PCR analysis. (**b**) Real-time PCR results showed ∼ 70-fold more *hbbe3* mRNA was accumulated in *rps19* mutant embryos than control embryos. (**c**) Western blot results indicated protein levels of both *hbbe1* and *hbbe3* were dramatically decreased in *rps19* mutant embryos at 3 dpf. Histograms represented quantification of western blots. (**d**) Decreased *mpx* mRNA was detected in *rps19* mutants compared with control embryos. (**e**) Equal to more *mpx* protein was produced in *rps19* mutants than control embryos at 3 dpf. Histograms represented quantification of western blots. Actin acts as a loading control. The results are representative for three independent experiments. $*P < 0.05$; $***P < 0.001$; Student's *t*-test

Protein production in erythroid cells is also decreased in *rpl11* mutants. To assess protein production in erythroid cells in *rpl11* mutants, we bred the transgenic lines into the *rpl11* mutant line. As expected, approximately two- to fivefold more *mCherry* mRNA was detected by real-time PCR in mCherry-positive *rpl11* mutant embryos compared with siblings at 3 dpf (Figure 6a). However, less mCherry protein was produced in *rpl11* mutants (Figures 6b and c). This suggests that protein production in erythroid cells was also inhibited in *rpl11* mutants. Similar with *rps19* mutants, the dissociation of RNA and protein levels of *mCherry* was

more obvious in *rpl11* mutants of mCherry control transgenic line.

To exclude the possibility that general protein translational defect led to erythroid protein production deficit, we examined the translational rates in both models. Cells from wild-type control embryos and *rps19* mutants were respectively starved by culturing in methionine and cysteine-free medium. Following starvation, ^{35}S-labeled methionine and cysteine were incorporated into those cells and the radioactivity was measured. As shown in Supplementary Figure S4a, the global translation rate was reduced only ∼ 40% in *rps19*

mutants compared to the control group, which was much less significant than the reduction of erythroid-specific mCherry protein levels in *rps19* transgenic mutants (~70–85%).

We performed the same experiments with *rpl11* mutants. Results showed that general translation rate was comparable between control embryos and *rpl11* mutants
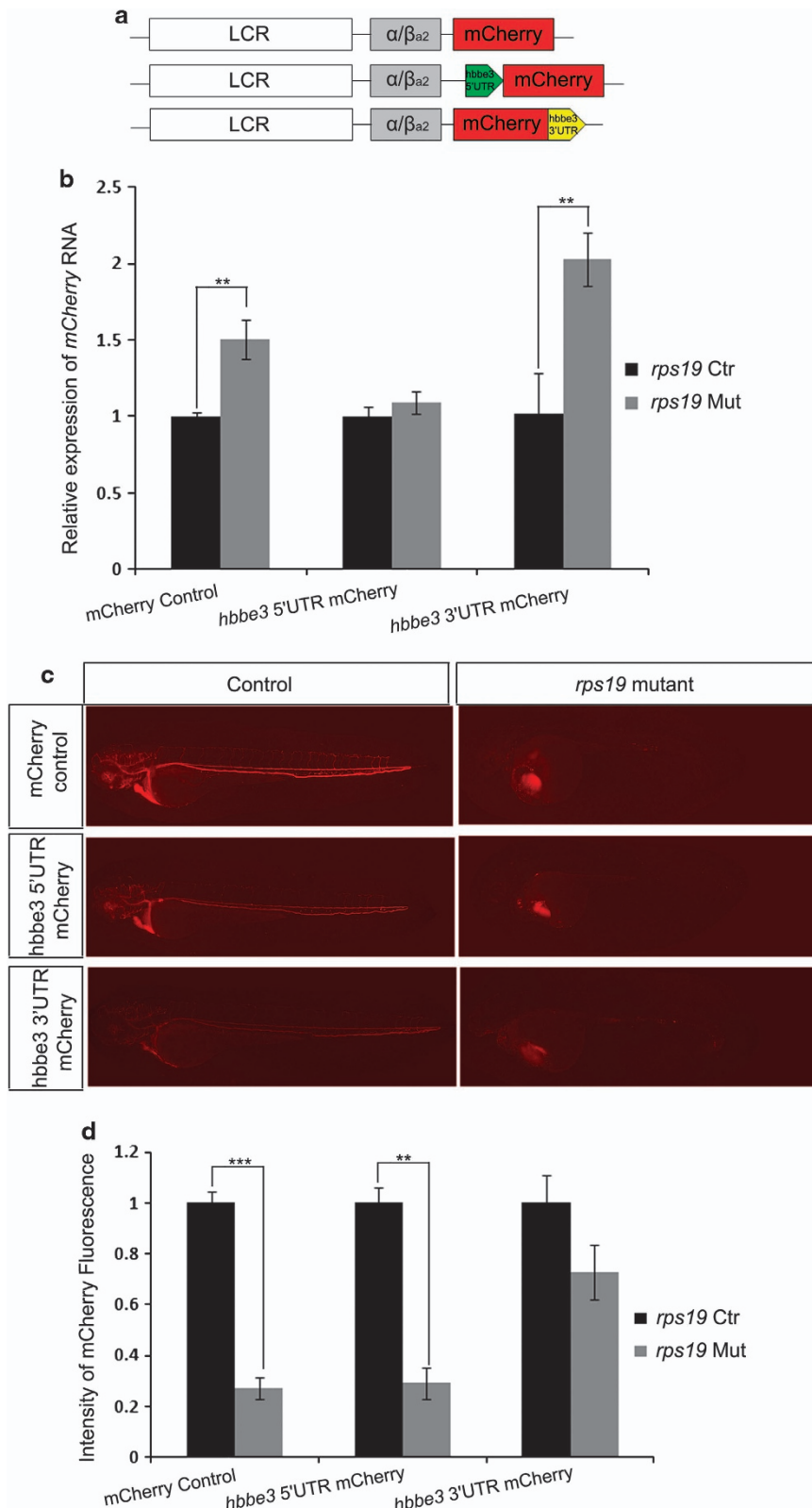
(Supplementary Figure S4b). These findings suggest that the erythroid protein production defect we observed in both *rps19* mutants and *rpl11* mutants was not simply contributed by general translational defect.

Meanwhile, expression of gata1, which is essential for differentiation of erythroid progenitor cells, was unaffected or slightly reduced in both *rps19* mutants and *rpl11* mutants, with more *gata1* mRNA was detected in both mutant models at
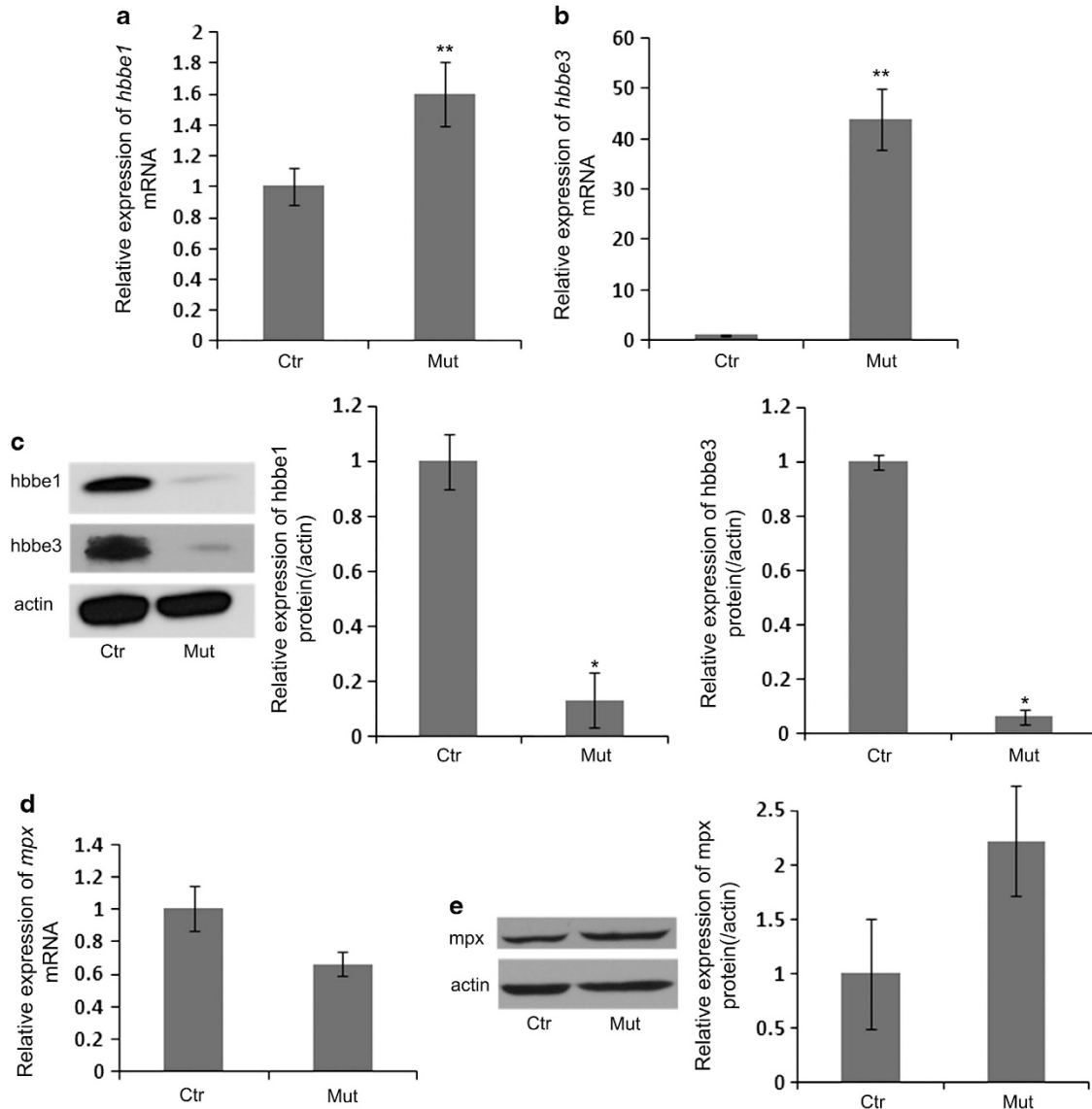
Figure 5 RNA and protein levels of *globin* genes are also dissociated in *rpl11* mutants. (**a**) mRNA expression of *hbbe1* was increased to 1.5-fold in *rpl11* mutant embryos at 3 dpf by real-time PCR analysis. (**b**) Real-time PCR results showed ∼50-fold more *hbbe3* mRNA was accumulated in *rpl11* mutant embryos compared to control embryos. (**c**) Western blot results indicated dramatic decrease of hbbe1 and hbbe3 protein levels in *rpl11* mutants at 3 dpf. Histograms represented quantification of western blots. (**d**) Slightly decreased *mpx* mRNA was detected in *rpl11* mutants compared with control embryos. RNA was pooled from 10 embryos. (**e**) Mpx protein was detected by western blot. Expression of mpx protein was comparable between *rpl11* mutant embryos and siblings, or more mpx protein was detected in *rpl11* mutant embryos than siblings. Histograms represented quantification of western blots. Actin acts as a loading control. The results are representative for three independent experiments. $*P<0.05$; $**P<0.01$; Student's *t*-test

Figure 4 Protein production in erythroid cells is decreased in *rps19* mutants. (**a**) Representation of the constructs for generating transgenic zebrafish lines. Zebrafish erythroid-specific regulatory region – locus control region (LCR) as well as a portion of α/β_{a2} bidirectional proximal promoter was cloned into mCherry reporter constructs. 5′UTR or 3′UTR of *hbbe3* was also included into one of the constructs. (**b**) Real-time PCR results showed more or the same amount of mCherry RNA in mCherry-positive *rps19* mutant embryos compared with control group at 3 dpf. (**c**) Representative images of mCherry-positive embryos of different transgenic lines at 3 dpf. Less mCherry expression was observed in *rps19* mutants than control embryos in all three transgenic lines. Lateral view shown with anterior to the left. (**d**) Quantification of intensity of mCherry fluorescence in the embryos shown in **c**. Intensity of mCherry fluorescence shown in *rps19* mutant mCherry control transgenic embryos was only 27% of the siblings. Approximately, 30% of mCherry fluorescence was exhibited by *rps19* mutant hbbe3 5′UTR mCherry transgenic embryos, compared with the control embryos. The results are representative for three independent experiments. $***P<0.001$; $**P<0.01$; Student's *t*-test
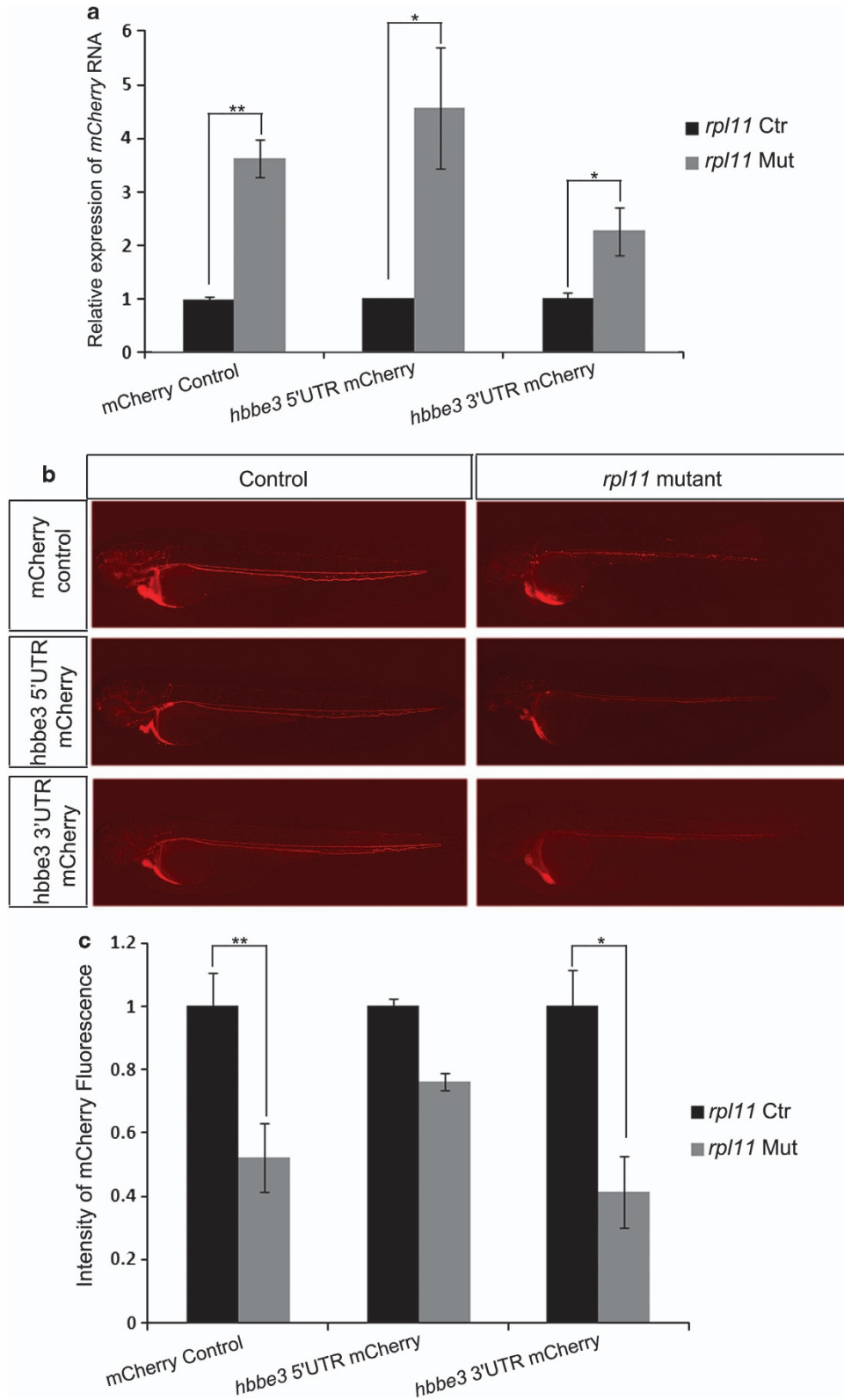
Figure 6 Protein production in erythroid cells is also decreased in *rpl11* mutants. (**a**) Real-time PCR results showed more than twofolds of *mCherry* RNA accumulated in mCherry-positive *rpl11* mutant embryos compared with control groups at 3 dpf. (**b**) Representative images of mCherry-positive embryos of different transgenic lines at 3 dpf. Less mCherry expression was observed in *rpl11* mutants than control embryos. Lateral view shown with anterior to the left. (**c**) Quantification of intensity of mCherry fluorescence in the embryos shown in **b**. Intensity of mCherry fluorescence shown in *rpl11* mutant mCherry control transgenic embryos was ∼50% of the siblings. Approximately, 40% of mCherry fluorescence was exhibited by *rpl11* mutant hbbe3 3′UTR mCherry transgenic embryos, compared with the control embryos. The results are representative for three independent experiments. **$P < 0.01$; *$P < 0.05$; Student's *t*-test

3 dpf (Supplementary Figure S5a-d). This indicates the production of erythroid progenitors is probably unaffected. In addition, no significant difference was detected in the percentage of mCherry-positive cells in both *rps19* and *rpl11* mutant transgenic embryos from *Tg (LCR: mCherry)* at 3 dpf (Supplementary Figure S5e and f), suggesting that the defects of protein production in erythroid cells were not simply due to reduction of erythroid cell numbers.

Furthermore, to exclude any adverse effect of blood circulation on the defects of gene expression in erythroid cells in both ribosomal mutation models, we injected rhodamine fluorescent dye into heart and analyzed the status of circulation at 3 dpf. Results showed that circulation was intact in both *rps19* and *rpl11* mutants (Supplementary Figure S6). This indicates that deficits of protein production in erythroid cells observed in both ribosomal mutation models were not caused by impaired circulation.

Taken together, for the first time we uncovered an RNA/protein production dissociation of *globin* genes in both *rps19* and *rpl11* mutants. Furthermore, defective protein synthesis in erythroid cells was seen in both *rps19* and *rpl11* mutants. This indicates that accumulative defects of protein production in erythroid cells probably contribute to the reduction of globin

proteins, which leads to the blood-specific defects in DBA patients.

L-leucine treatment alleviates the decreased protein production of *globin* genes and partially rescues the anemic phenotype in both *rps19* and *rpl11* mutants.

L-Leucine is known to increase protein synthesis in skeletal muscle.[33] Protein synthesis was increased in DBA-derived cells after treatment with L-leucine.[22] L-Leucine treatment improved anemia in several animal models with ribosomal protein deficiency.[34,35] To evaluate the effect of L-leucine treatment on our disease models, we treated both *rps19* and *rpl11* mutants with L-leucine. Compared to control, addition of L-leucine improved part of the developmental defects, including edema, in both *rps19* and *rpl11* mutants (Figures 7a and 8a). To assess if L-leucine treatment plays a role in the protein synthesis defect of *globin* genes described above, we analyzed expression of *hbbe3*. Real-time PCR results showed that expression of *hbbe3* at mRNA level was comparable between control mutant embryos and mutant embryos raised in L-leucine in both *rps19* and *rpl11* mutants at 3 dpf (Figures 7b and 8b). However, protein level of hbbe3 was significantly increased in mutant embryos
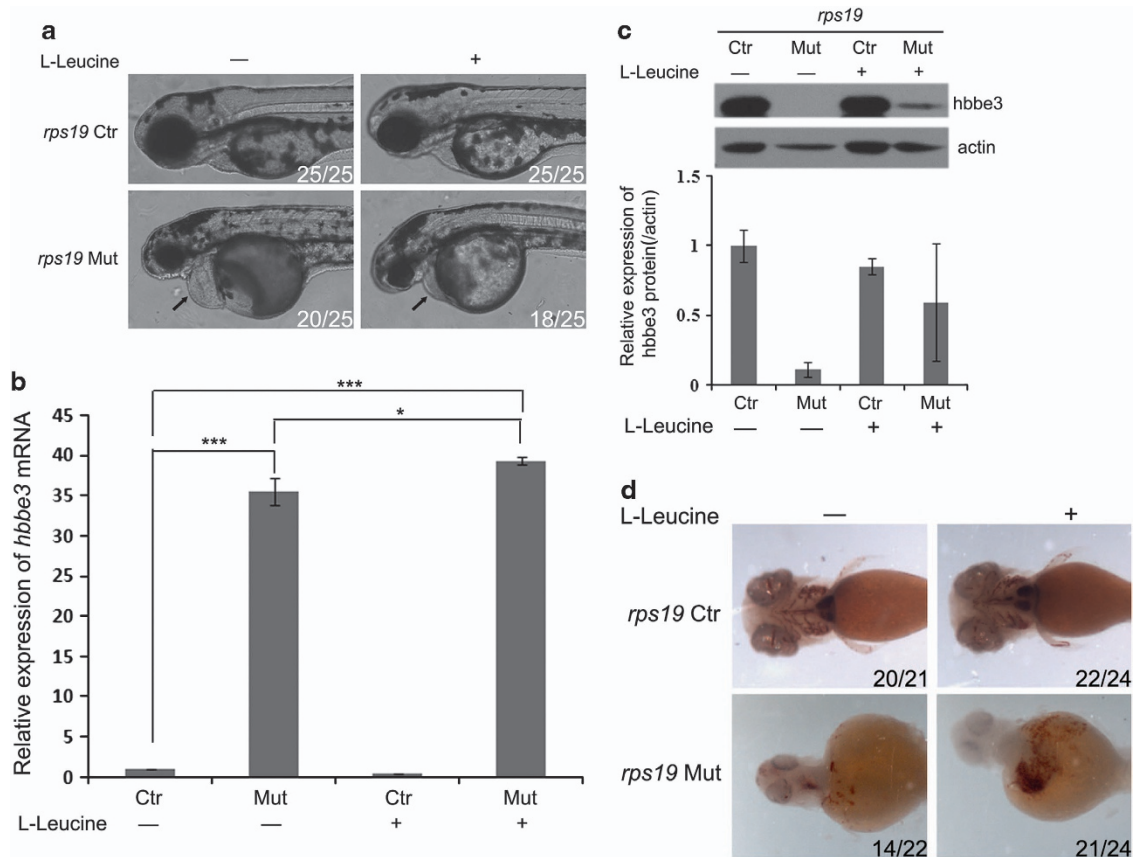
Figure 7 L-Leucine treatment alleviates the protein production defect of *globin* gene and partially rescues the anemic phenotype in *rps19* mutant embryos. (**a**) *Rps19* mutant embryos raised in fish water developed severe edema (black arrow) at 3 dpf, while the edema was improved after L-leucine treatment in *rps19* mutant embryos (black arrow). L-Leucine had no effect on control embryos. Lateral view with anterior to the left. (**b**) Real-time PCR results showed that mRNA expression of *hbbe3* was slightly increased in *rps19* mutant embryos after addition of L-leucine compared with mutant embryos in fish water at 3 dpf. (**c**) hbbe3 protein expression was detected by western blot analysis. Expression of hbbe3 was dramatically increased by treatment of L-leucine in *rps19* mutant embryos at 3 dpf. Histograms represented quantification of western blots. Actin acts as a loading control. (**d**) More hemoglobin staining signals were detected in *rps19* mutant embryos treated with L-leucine than the mutant embryos raised in fish water at 4 dpf. Ventral view with anterior to the left. The results are representative for two independent experiments. *$P < 0.05$; ***$P < 0.001$; Student's *t*-test
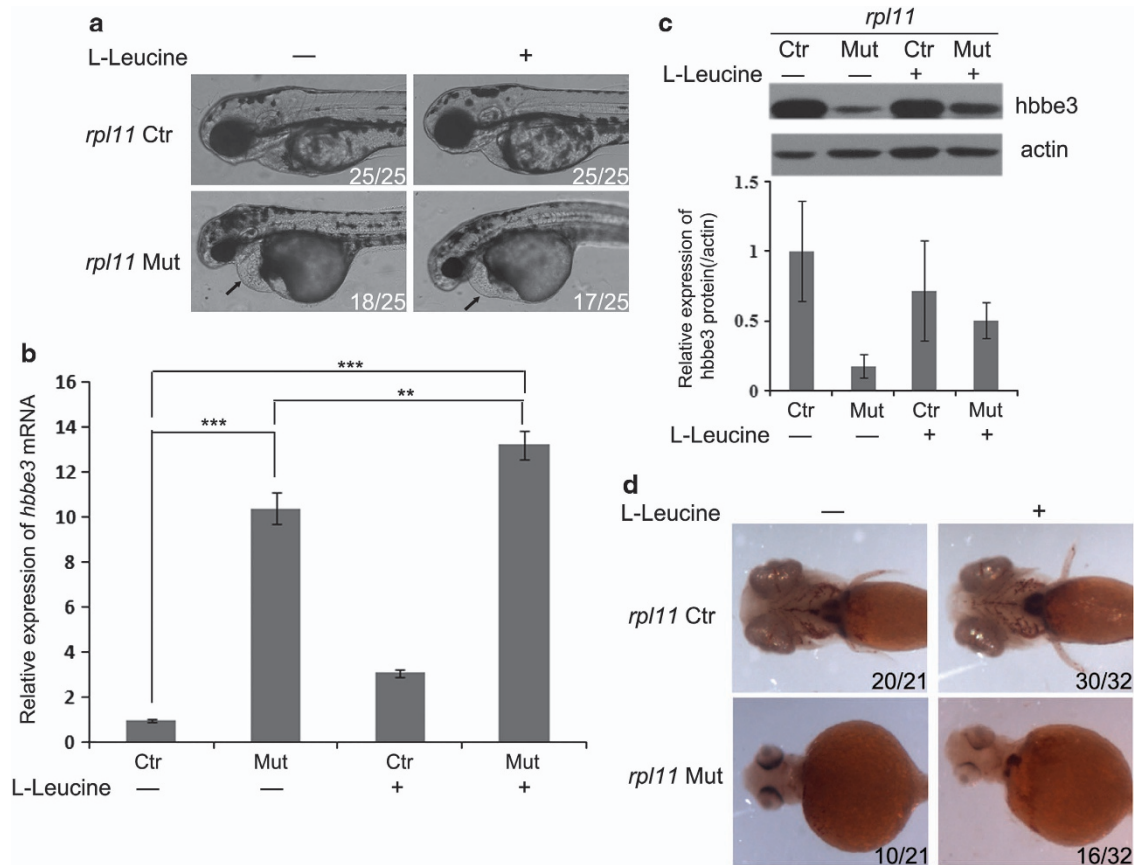
Figure 8 L-Leucine treatment improves the protein production defect of *globin* gene and partially rescues the anemic phenotype in *rpl11* mutant embryos. (**a**) Similar with *rps19* mutant embryos, *rpl11* mutant embryos raised in fish water developed severe edema (black arrow) at 3 dpf, while the edema was improved after L-leucine treatment in *rpl11* mutant embryos (black arrow). Lateral view with anterior to the left. (**b**) mRNA expression of *hbbe3* was slightly increased in *rpl11* mutant embryos after addition of L-leucine compared with mutant embryos in fish water at 3 dpf by real-time PCR analysis. (**c**) hbbe3 protein expression was detected by western blot analysis. Expression of hbbe3 was dramatically increased after treatment of L-leucine in *rpl11* mutant embryos at 3 dpf. Histograms represented quantification of western blots. Actin acts as a loading control. (**d**) Similar with the results of *rps19* mutants, more hemoglobin staining signals were detected in *rpl11* mutant embryos treated with L-leucine than the mutant embryos raised in fish water at 4 dpf. Ventral view with anterior to the left. The results are representative for two independent experiments. **$P < 0.01$; ***$P < 0.001$; Student's *t*-test

treated with L-leucine compared to control regardless of *rps19* mutation or *rpl11* mutation. Meanwhile, protein level of hbbe3 in wild-type and heterozygous siblings was not altered by the addition of L-leucine (Figures 7c and 8c). To address if increasing the protein production of *globin* gene could lead to the improvement of anemia observed in mutants, we performed *o*-dianisidine staining for both *rps19* and *rpl11* mutants. We found that L-leucine treatment partially improved the anemic phenotype in both *rps19* and *rpl11* mutants (Figures 7d and 8d). Overall, our *rps19* model, as well as *rpl11* mutants is responsive to L-leucine treatment. Anemia was improved in both *rps19* and *rpl11* mutants with L-leucine treatment, similar to human DBA patients following L-leucine treatment.[36] Our zebrafish *rps19* mutant line appears promising as a useful model towards better understanding the mechanistic defects in DBA and also aids in the discovery of novel therapeutics to treat the disease.

Discussion

In this study, we generated *rps19* mutant zebrafish lines using TALENs. As reported in DBA patients, *rps19* mutants exhibited

hematopoietic phenotypes and developed anemia associated with activation of the *p53* signaling pathway. We therefore believe that this *rps19* mutant zebrafish should serve as a useful animal model to study the pathogenesis of DBA.

Mechanism of erythroid failure in DBA. *RPS19* was the first identified gene whose mutation is currently identified in 25% of DBA patients.[2] To date, mutations in at least other nine ribosomal genes, including *RPL11*, have been reported in DBA patients.[12] The ribosomal stress and upregulation of the *P53* signaling pathway caused by haploinsufficiency of ribosomal proteins are thought to lead to the clinical features of DBA.[17,18] According to data from *in vitro* experiments, the specific erythropoietic defects in DBA were thought to be attributed to the hypersensitivity of erythroblasts to the upregulation of TP53[17] and/or the high demand for ribosome synthetic rates of rapidly proliferative erythroid cells.[26] Other hypotheses, including reduced translation of some specific transcripts essential for erythropoiesis[23] also exist. Recently, a mutation of *GATA1*, an erythroid-specific transcription factor, was identified in two siblings and another unrelated DBA patients.[37] Splicing of *GATA1* was impaired by the

mutation. Mutation of the erythroid-specific gene may contribute to the erythroid-specific phenotype of DBA. However, it remains controversial whether these patients are real DBA cases, because their clinical manifestations did not meet all of the clinical diagnostic criteria for DBA.[1]

For the first time, our *in vivo* data demonstrated translational defects with globin genes in both *rps19* and *rpl11* mutants, despite increased or similar transcriptional levels. More importantly, we found that translation was disrupted specifically in erythroid cells in both *rps19*- and *rpl11*-deficient zebrafish. This is further supported by observations showing translation of a neutrophil-specific gene was largely unaffected in both mutant zebrafish. We speculate that protein synthesis defects may affect the survival of erythroid cells, for instance, through the activation of cell-cycle arrest and apoptosis in erythroid cells.[38] These findings will advance our understanding toward the mechanisms of erythroid failure in DBA.

Extra-ribosomal functions of ribosomal proteins. Some ribosomal proteins have been reported to have unexpected functions outside of the ribosome (extra-ribosomal functions). In eukaryotic cells, RPL2, RPL30, RPS14, and RPS28 were reported to function by binding to their own transcripts or some other mechanisms to perform regulation of ribosomal protein production.[39–42] RPL5, RPL11 and 5S rRNA were found to interact with MDM2, which is responsible for regulating the *p53* signaling pathway via the ubiquitination and degradation of *p53*.[43–46] RPL13a was reported to be involved in a transcript-specific translational control mechanism. RPL13a can be phosphorylated and released from the 60S ribosomal subunit in response to interferon-γ. Released RPL13a specifically binds the 3′UTR interferon-gamma-activated inhibitor of translation element of its target mRNAs and inhibits translation.[47]

Recently, analysis of *RPL38*'s function provided insight into the specialized ribosome activity controlled by ribosomal proteins. *Rpl38* was found to be deleted in tail short (Ts) mice. *Rpl38* had higher expression in somites and neural tube, where Ts mice showed tissue-specific phenotype. Interestingly, translation of 8 of the 39 homeobox (Hox) genes, which are essential for the morphological development along the axial skeleton was reduced in Ts mice. The tissue-specific expression pattern of *Rpl38* correlated with the specific phenotype observed in Ts mice.[48] These findings suggested the possibility that increased expression of specific ribosomal proteins in unique tissues might lead to the heterogeneous ribosomes in the distinguished cell tissues by specificities in translating distinct classes of mRNAs. However, this is not the case for *rps19* or *rpl11*. We checked the expression patterns of *rps19*, *rpl11* and *rpl38* in zebrafish using RNA whole-mount *in situ* hybridization. All of them had ubiquitous expression during embryonic development (data not shown). This suggested that the erythroid-specific translational defect exhibited by *rps19*- and *rpl11*-deficient zebrafish was not attributed to the tissue-specific expression of *rps19* and *rpl11*. It is possible that some erythroid-specific ribosome-associated factors, which have interactions with *rps19* and/or *rpl11* may mediate this event by inhibiting the translation of erythroid genes. Application of ribosomal profiling strategy will put forward some candidates for this issue.

In summary, utilizing TALENs we generated *rps19* mutants in zebrafish. Similar with DBA patients, *rps19* mutants had hematopoietic defects and developed anemia; thus, serving as a novel DBA model. Using the newly generated line, we reported the RNA and protein production dissociation of *globin* genes in *rps19* mutant and confirmed similar findings in *rpl11* mutant. Further analysis demonstrates that the dissociation may result from reduced protein production in erythroid cells in *rps19*- or *rpl11*-deficient zebrafish. Expression, however, of neutrophil gene was unaffected. For the first time, our *in vivo* data suggested that the erythroid defects in DBA may be caused by the decreased protein production of erythroid cells in patients. Recently, L-leucine was found to improve the anemia of *rps19*-deficient zebrafish by activating the mTOR pathway;[34] however, the underlying mechanism is still under investigation. Our results showed L-leucine treatment alleviated the protein production defects of *globin* gene and partially rescued the anemic phenotype in both *rps19* and *rpl11* mutants. Based on our findings, L-leucine may work through activating translation of erythroid cells. Our findings will aid in the understanding of clinical manifestation of DBA. Additionally, the newly derived *rps19* mutants promise to be useful for investigating the basis for erythroid defects and serve as a tool to carry out therapeutic screens to develop much-needed treatments toward DBA.

Materials and Methods

Zebrafish lines and maintenance. Zebrafish (*Danio rerio*) was raised and maintained under standard laboratory conditions at 28.5°C. All the three constructs for transgenic fish were generated utilizing the Gateway system (Invitrogen, Carlsbad, CA, USA). Approximately, 30 pg of the constructs together with 15 pg Tol2 mRNA were injected into the embryos at one-cell stage; 5 ng of *p53* ATG morpholino[49] was injected into the embryos at one-cell stage for *p53* rescue experiment.

Generating *rps19* mutant by TALENs. Design of TALENs target site using the online service at: https://tale-nt.cac.cornell.edu/node/add/talen. The sequence-specific TAL effector repeats against the right and left arms (Figure 1a) were constructed using the 'unit assembly' method.[27] mRNAs encoding left and right TALENs were synthesized *in vitro* by using the T7 mMessage Machine kit (Ambion, Austin, TX, USA) and purified using a kit from Invitrogen according to the manufactures' instructions. mRNAs were mixed at the ratio of 1 : 1 and co-injected into wild-type zebrafish embryos at one-cell stage at 100 pg mRNA/embryo as the final dose. Every three injected and morphologically normal embryos were mixed at 24 hpf to isolate genomic DNA followed by PCR amplification. Total of 24 embryos from each injection group were used to evaluate the efficiency of the generated TALENs. A 305 bp genomic DNA fragment containing the target site was PCR amplified from injected and/or uninjected control embryos. Primers used for this PCR were: forward: 5′-AAGTCCTGGTCTTGGGACAA-3′; reverse: 5′-G GAATGGACGAAAGTTACACTG-3′. The PCR products were denatured, annealed and digested with Transgenomic Surveyor Mutation Detection Kit (Transgenomic, Omaha, NE, USA) for Standard Gel Electrophoresis (catalog number: 706020) by following the manufacturer's instruction. The digested PCR products were separated by electrophoresis on 2% agarose gel and/or 0.8% PAGE gel.

Real-time PCR. RNA was isolated from 7–15 embryos at 3 dpf using Trizol (Invitrogen) according to the manufacturer's protocol; 2 ug of total RNA was used for cDNA synthesis by reverse transcription using Oligo(dT)$_{12–18}$ (Invitrogen). Real-time PCR was performed using FastStart Universal SYBR Green MasterMix (Roche Diagnostics, Indianapolis, IN, USA) and a MyiQ Single-Color PCR thermal cycler (Biorad, Hercules, CA, USA). Real-time PCR primers used for *p53* signaling pathway were from previous literature.[19] Sequences of real-time PCR primers for *hbbe1*: RTF: 5′-TTGTGTGGACAGACTTCGAGA-3′ and RTR: 5′-TCAGCATAG GTGGCCTTGAT-3′; for *hbbe3*: RTF: 5′-ATGGTTGTGTGGACAGCTG-3′ and RTR: 5′-ATTATCCATGTTGTTGAGAGC-3′; for *mpx*: RTF3: 5′-GGGGCAGAAGAAGA

AAGTCC-3′ and RTR3: 5′-CCCTTGCTAAACTCTCATCTC-3′; for *rps19*: RTF1: 5′-ATGCCAGGTGGTGTAACAGT-3′ and RTR1: 5′-GTCATAGAGCCCACGC CAAC-3′; for *mCherry*: RTF1: 5′-GCGGCACCAACTTCCCCTCC-3′ and RTR1: 5′-TCGGCGCGCTCGTACTGTTC-3′; for *gata1*: RTF: 5′-TGAATGTGTGAAT TGTGGTG-3′ and RTR: 5′-ATTGCGTCTCCATAGTGTTG-3′.[50]

Whole-mount *in situ* hybridization. Whole-mount *in situ* hybridization was conducted as described[51] using *c-myb*, *mpx*, *rag1*,[49] *hbbe1*, and *hbbe3*[52] riboprobes.

Whole-mount *o*-dianisidine staining. Hemoglobin was measured by whole-mount *o*-dianisidine staining as described previously.[49]

Western blot analysis. Approximately, 15–20 embryos were rinsed and lysed in lysis buffer. Protein concentration was measured with bicinchoninic acid Protein Assay Kit (Thermo Scientific, Rockford, IL, USA) or NanoDrop 1000 Spectro-photometer (Thermo Scientific); 20–40 mg of total protein was employed for western blot analysis. Procedure of western blot was described previously.[30] Primary antibodies for hbbe1 (AnaSpec, Fremont, CA, USA), mpx (AnaSpec), gata1a (Anaspec), and actin (Sigma, St. Louis, MO, USA) and horseradish peroxidase-linked secondary antibodies (GE Healthcare, Uppsala, Sweden) were used. Synthetic peptide corresponding to the N-terminal region of zebrafish hbbe3 was produced for generating customized primary antibody for hbbe3 (AnaSpec). Western blot results were quantified using ImageJ which was downloaded from NIH website.

Analysis of mCherry fluorescence. For each group, 28–30 embryos were photoed under fluorescent microscope (Zeiss, Oberkochen, Germany) at 3 dpf. The fluorescence of mCherry was analyzed using ImageJ. Images were opened using ImageJ software. The same thresholds for both control and mutant embryos were set up to reflect the expression of mCherry throughout the whole embryo. Area, minimum and maximum gray value, integrated density, and mean gray value were measured. Measurements were set as limit to threshold. The whole embryo was measured. The value of area and mean intensity was multiplied to get the intensity of mCherry fluorescence for each embryo.

L-Leucine treatment. Embryos were divided into two groups at 10 hpf. One group was raised in fish water with 100 mM L-leucine (Sigma), and the other group was raised in fish water. Embryos were collected for the following experiments at 3 and 4 dpf.

Analysis of general translation rate. Overall, 40–80 embryos at 3 dpf were homogenized and dissociated into single cells with 0.25% Trypsin-EDTA (Invitrogen). Cells were counted. Comparable amount of cells ($\sim 4 \times 10^5$ cells) from each group were used. Cells were rinsed twice with methionine-free and cysteine-free DMEM (Invitrogen) followed by incubation in the same medium at 28.5 °C for one hour. S^{35}-labeled methionine and cysteine (Perkin Elmer, Santa Clara, CA, USA) were added into the culture medium at 10 μCi/ml. After incubation for another 1 h, cells were collected by centrifuging at 4 °C for 5 min. Cells were rinsed twice with ice-cold phosphate-buffered saline (PBS). The cells were resuspended in 100 μl lysis buffer containing 50 mM Tris-HCl (pH 7.5), 150 mM NaCl, 1% Triton X-100, and proteinase inhibitor cocktail (Roche Diagnostics). Proteins in the lysate were precipitated by adding trichloroacetic acid (Sigma-Aldrich) and incubated for 30 min on ice. Proteins were recovered by vacuum filtration on cellulose filters (Whatman, Uppsala, Sweden) and dried out. The filters were dissolved with scintillation cocktail, and radioactivity from samples were measured with Liquid Scintillation Analyzer (Perkin Elmer). Meanwhile, protein concentration was measured using NanoDrop 1000 Spectrophotometer (Thermo Scientific).

Examination of circulation by angiocardiography. Embryos at 3 dpf were treated with $\times$ 1 tricaine. After injecting rhodamine fluorescent dye into their hearts, embryos were immediately observed and pictured with fluorescent microscope (Zeiss); 8–10 embryos for each group were injected and observed.

Analysis of percentage of mCherry-positive cells. Equal number (30–50) of transgenic embryos at 3 dpf were homogenized and dissociated into single cells with 0.25% Trypsin-EDTA (Invitrogen). Cells were rinsed twice and resuspended in $\times$ 1 PBS. The percentage of mCherry-positive cells was analyzed using BD LSRFortessa cell analyzer (BD Biosciences, San Jose, CA, USA).

Author Contributions

YZ, KM, BZ, and SL designed the experiments. YZ, ZY, and KM conducted the experiments. YZ, BZ, and SL analyzed the data. YZ, JE, BZ, and SL wrote the paper.

1. Horos R, von Lindern M. Molecular mechanisms of pathology and treatment in Diamond Blackfan Anaemia. *Br J Haematol* 2012; **159**: 514–527.
2. Draptchinskaia N, Gustavsson P, Andersson B, Pettersson M, Willig TN, Dianzani I *et al.* The gene encoding ribosomal protein S19 is mutated in Diamond-Blackfan anaemia. *Nat Genet* 1999; **21**: 169–175.
3. Willig TN, Gazda H, Sieff CA. Diamond-Blackfan anemia. *Curr Opin Hematol* 2000; **7**: 85–94.
4. Campagnoli MF, Garelli E, Quarello P, Carando A, Varotto S, Nobili B *et al.* Molecular basis of Diamond-Blackfan anemia: new findings from the Italian registry and a review of the literature. *Haematologica* 2004; **89**: 480–489.
5. Vlachos A, Federman N, Reyes-Haley C, Abramson J, Lipton JM. Hematopoietic stem cell transplantation for Diamond Blackfan anemia: a report from the Diamond Blackfan Anemia Registry. *Bone Marrow Transplant* 2001; **27**: 381–386.
6. Gazda HT, Grabowska A, Merida-Long LB, Latawiec E, Schneider HE, Lipton JM *et al.* Ribosomal protein S24 gene is mutated in Diamond-Blackfan anemia. *Am J Hum Genet* 2006; **79**: 1110–1118.
7. Cmejla R, Cmejlova J, Handrkova H, Petrak J, Pospisilova D. Ribosomal protein S17 gene (RPS17) is mutated in Diamond-Blackfan anemia. *Hum Mutat* 2007; **28**: 1178–1182.
8. Farrar JE, Vlachos A, Atsidaftos E, Carlson-Donohoe H, Markello TC, Arceci RJ *et al.* Ribosomal protein gene deletions in Diamond-Blackfan anemia. *Blood* 2011; **118**: 6943–6951.
9. Farrar JE, Nater M, Caywood E, McDevitt MA, Kowalski J, Takemoto CM *et al.* Abnormalities of the large ribosomal subunit protein, Rpl35a, in Diamond-Blackfan anemia. *Blood* 2008; **112**: 1582–1592.
10. Gazda HT, Sheen MR, Vlachos A, Choesmel V, O'Donohue MF, Schneider H *et al.* Ribosomal protein L5 and L11 mutations are associated with cleft palate and abnormal thumbs in Diamond-Blackfan anemia patients. *Am J Hum Genet* 2008; **83**: 769–780.
11. Doherty L, Sheen MR, Vlachos A, Choesmel V, O'Donohue MF, Clinton C *et al.* Ribosomal protein genes RPS10 and RPS26 are commonly mutated in Diamond-Blackfan anemia. *Am J Hum Genet* 2010; **86**: 222–228.
12. Gazda HT, Preti M, Sheen MR, O'Donohue MF, Vlachos A, Davies SM *et al.* Frameshift mutation in p53 regulator RPL26 is associated with multiple physical abnormalities and a specific pre-ribosomal RNA processing defect in diamond-blackfan anemia. *Hum Mutat* 2012; **33**: 1037–1044.
13. Choesmel V, Bacqueville D, Rouquette J, Noaillac-Depeyre J, Fribourg S, Cretien A *et al.* Impaired ribosome biogenesis in Diamond-Blackfan anemia. *Blood* 2007; **109**: 1275–1283.
14. Flygare J, Aspesi A, Bailey JC, Miyake K, Caffrey JM, Karlsson S *et al.* Human RPS19, the gene mutated in Diamond-Blackfan anemia, encodes a ribosomal protein required for the maturation of 40S ribosomal subunits. *Blood* 2007; **109**: 980–986.
15. Idol RA, Robledo S, Du HY, Crimmins DL, Wilson DB, Ladenson JH *et al.* Cells depleted for RPS19, a protein associated with Diamond Blackfan Anemia, show defects in 18S ribosomal RNA synthesis and small ribosomal subunit production. *Blood Cells Mol Dis* 2007; **39**: 35–43.
16. Robledo S, Idol RA, Crimmins DL, Ladenson JH, Mason PJ, Bessler M. The role of human ribosomal proteins in the maturation of rRNA and ribosome production. *RNA* 2008; **14**: 1918–1929.
17. Dutt S, Narla A, Lin K, Mullally A, Abayasekara N, Megerdichian C *et al.* Haploinsufficiency for ribosomal protein genes causes selective activation of p53 in human erythroid progenitor cells. *Blood* 2011; **117**: 2567–2576.
18. Jaako P, Flygare J, Olsson K, Quere R, Ehinger M, Henson A *et al.* Mice with ribosomal protein S19 deficiency develop bone marrow failure and symptoms like patients with Diamond-Blackfan anemia. *Blood* 2011; **118**: 6087–6096.

19. Danilova N, Sakamoto KM, Lin S. Ribosomal protein S19 deficiency in zebrafish leads to developmental abnormalities and defective erythropoiesis through activation of p53 protein family. *Blood* 2008; **112**: 5228–5237.

20. Torihara H, Uechi T, Chakraborty A, Shinya M, Sakai N, Kenmochi N. Erythropoiesis failure due to RPS19 deficiency is independent of an activated Tp53 response in a zebrafish model of Diamond-Blackfan anaemia. *Br J Haematol* 2011; **152**: 648–654.

21. Taylor AM, Zon LI. Modeling Diamond Blackfan anemia in the zebrafish. *Semin Hematol* 2011; **48**: 81–88.

22. Cmejlova J, Dolezalova L, Pospisilova D, Petrtylova K, Petrak J, Cmejla R. Translational efficiency in patients with Diamond-Blackfan anemia. *Haematologica* 2006; **91**: 1456–1464.

23. Horos R, Ijspeert H, Pospisilova D, Sendtner R, Andrieu-Soler C, Taskesen E *et al*. Ribosomal deficiencies in Diamond-Blackfan anemia impair translation of transcripts essential for differentiation of murine and human erythroblasts. *Blood* 2012; **119**: 262–272.

24. Rey MA, Duffy SP, Brown JK, Kennedy JA, Dick JE, Dror Y *et al*. Enhanced alternative splicing of the FLVCR1 gene in Diamond Blackfan anemia disrupts FLVCR1 expression and function that are critical for erythropoiesis. *Haematologica* 2008; **93**: 1617–1626.

25. Quigley JG, Burns CC, Anderson MM, Lynch ED, Sabo KM, Overbaugh J *et al*. Cloning of the cellular receptor for feline leukemia virus subgroup C (FeLV-C), a retrovirus that induces red cell aplasia. *Blood* 2000; **95**: 1093–1099.

26. Sieff CA, Yang J, Merida-Long LB, Lodish HF. Pathogenesis of the erythroid failure in Diamond Blackfan anaemia. *Br J Haematol* 2010; **148**: 611–622.

27. Huang P, Xiao A, Zhou M, Zhu Z, Lin S, Zhang B. Heritable gene targeting in zebrafish using customized TALENs. *Nat Biotechnol* 2011; **29**: 699–700.

28. Danilova N, Kumagai A, Lin J. p53 upregulation is a frequent response to deficiency of cell-essential genes. *PLoS One* 2010; **5**: e15938.

29. Taylor AM, Humphries JM, White RM, Murphey RD, Burns CE, Zon LI. Hematopoietic defects in rps29 mutant zebrafish depend upon p53 activation. *Exp Hematol* 2012; **40**: 228–237; e225.

30. Danilova N, Sakamoto KM, Lin S. Ribosomal protein L11 mutation in zebrafish leads to haematopoietic and metabolic defects. *Br J Haematol* 2011; **152**: 217–228.

31. Ganis JJ, Hsia N, Trompouki E, de Jong JL, DiBiase A, Lambert JS *et al*. Zebrafish globin switching occurs in two developmental stages and is controlled by the LCR. *Dev Biol* 2012; **366**: 185–194.

32. Amsterdam A, Nissen RM, Sun Z, Swindell EC, Farrington S, Hopkins N. Identification of 315 genes essential for early zebrafish development. *Proc Natl Acad Sci USA* 2004; **101**: 12792–12797.

33. Kimball SR, Jefferson LS. New functions for amino acids: effects on gene transcription and translation. *Am J Clin Nutr* 2006; **83**: 500S–507S.

34. Payne EM, Virgilio M, Narla A, Sun H, Levine M, Paw BH *et al*. L-Leucine improves the anemia and developmental defects associated with Diamond-Blackfan anemia and del(5q) MDS by activating the mTOR pathway. *Blood* 2012; **120**: 2214–2224.

35. Jaako P, Debnath S, Olsson K, Bryder D, Flygare J, Karlsson S. Dietary L-leucine improves the anemia in a mouse model for Diamond-Blackfan anemia. *Blood* 2012; **120**: 2225–2228.

36. Pospisilova D, Cmejlova J, Hak J, Adam T, Cmejla R. Successful treatment of a Diamond-Blackfan anemia patient with amino acid leucine. *Haematologica* 2007; **92**: e66–e67.

37. Sankaran VG, Ghazvinian R, Do R, Thiru P, Vergilio JA, Beggs AH *et al*. Exome sequencing identifies GATA1 mutations resulting in Diamond-Blackfan anemia. *J Clin Invest* 2012; **122**: 2439–2443.

38. Gazda HT, Kho AT, Sanoudou D, Zaucha JM, Kohane IS, Sieff CA *et al*. Defective ribosomal protein gene expression alters transcription, translation, apoptosis, and oncogenic pathways in Diamond-Blackfan anemia. *Stem Cells* 2006; **24**: 2034–2044.

39. Presutti C, Ciafre SA, Bozzoni I. The ribosomal protein L2 in S. cerevisiae controls the level of accumulation of its own mRNA. *EMBO J* 1991; **10**: 2215–2221.

40. Eng FJ, Warner JR. Structural basis for the regulation of splicing of a yeast messenger RNA. *Cell* 1991; **65**: 797–804.

41. Fewell SW, Woolford Jr JL. Ribosomal protein S14 of Saccharomyces cerevisiae regulates its expression by binding to RPS14B pre-mRNA and to 18S rRNA. *Mol Cell Biol* 1999; **19**: 826–834.

42. Badis G, Saveanu C, Fromont-Racine M, Jacquier A. Targeted mRNA degradation by deadenylation-independent decapping. *Mol Cell* 2004; **15**: 5–15.

43. Marechal V, Elenbaas B, Piette J, Nicolas JC, Levine AJ. The ribosomal L5 protein is associated with mdm-2 and mdm-2-p53 complexes. *Mol Cell Biol* 1994; **14**: 7414–7420.

44. Lohrum MA, Ludwig RL, Kubbutat MH, Hanlon M, Vousden KH. Regulation of HDM2 activity by the ribosomal protein L11. *Cancer Cell* 2003; **3**: 577–587.

45. Dai MS, Shi D, Jin Y, Sun XX, Zhang Y, Grossman SR *et al*. Regulation of the MDM2-p53 pathway by ribosomal protein L11 involves a post-ubiquitination mechanism. *J Biol Chem* 2006; **281**: 24304–24313.

46. Zhang Y, Wolf GW, Bhat K, Jin A, Allio T, Burkhart WA *et al*. Ribosomal protein L11 negatively regulates oncoprotein MDM2 and mediates a p53-dependent ribosomal-stress checkpoint pathway. *Mol Cell Biol* 2003; **23**: 8902–8912.

47. Mazumder B, Sampath P, Seshadri V, Maitra RK, DiCorleto PE, Fox PL. Regulated release of L13a from the 60S ribosomal subunit as a mechanism of transcript-specific translational control. *Cell* 2003; **115**: 187–198.

48. Kondrashov N, Pusic A, Stumpf CR, Shimizu K, Hsieh AC, Xue S *et al*. Ribosome-mediated specificity in Hox mRNA translation and vertebrate tissue patterning. *Cell* 2011; **145**: 383–397.

49. Zhang Y, Morimoto K, Danilova N, Zhang B, Lin S. Zebrafish models for dyskeratosis congenita reveal critical roles of p53 activation contributing to hematopoietic defects through RNA processing. *PLoS One* 2012; **7**: e30188.

50. Bertrand JY, Kim AD, Teng S, Traver D. CD41+ cmyb+ precursors colonize the zebrafish pronephros by a novel migration route to initiate adult hematopoiesis. *Development* 2008; **135**: 1853–1862.

51. Thisse C, Thisse B, Schilling TF, Postlethwait JH. Structure of the zebrafish snail1 gene and its expression in wild-type, spadetail and no tail mutant embryos. *Development* 1993; **119**: 1203–1215.

52. Brownlie A, Hersey C, Oates AC, Paw BH, Falick AM, Witkowska HE *et al*. Characterization of embryonic globin genes of the zebrafish. *Dev Biol* 2003; **255**: 48–61.

Supplementary Information accompanies this paper on Cell Death and Disease website (http://www.nature.com/cddis)